Three-dimensional tracking of fluorescent nanoparticles with subnanometer precision by use of off-focus imaging

Michael Speidel, Alexandr Jonáš, and Ernst-Ludwig Florin

Cell Biology and Biophysics Programme, European Molecular Biology Laboratory, Meyerhofstrasse 1, D-69117 Heidelberg, Germany

Received August 5, 2002

We show that the position of a fluorescent nanoparticle can be measured in three dimensions with subnanometer precision and 100-ms temporal resolution by use of standard epifluorescence video imaging in off-focus mode. The particle can be tracked without feedback in a volume of at least 40 μm $\times$ 60 μm $\times$ 3 μm. With the technique presented, the structure–mobility relationship of 216-nm latex particle in a porous polymer network was studied in three dimensions. © 2003 Optical Society of America

OCIS codes: 100.2960, 180.2520, 350.5730.

Single-particle tracking (SPT) has become an invaluable tool in many scientific fields such as cell biology, soft-matter physics, and single-molecular research for studying, respectively, transport processes in cells,[1,2] interaction between colloidal particles[3] and the working cycles of molecular motors.[4] Among various tracking methods, tracking of fluorescent particles plays a central role because its specificity allows one to study processes in complex environments such as living cells. Moreover, using particles with different spectral signatures, molecular-scale distances between objects can be precisely measured, opening the possibility of following structural and dynamical aspects of complex nanostructures.[5]

Generally, it is required that the particle movement be followed in all three dimensions, because only complete position information ensures correct and unambiguous interpretation of the measured data (e.g., dynamics of a transport process). So far, such three-dimensional (3-D) high-precision fluorescent particle tracking has been achieved with specially designed epifluorescence microscopes,[6] 4-Pi microscopes,[7] and total internal reflection microscopes.[8] Despite these efforts, the precision is typically still in the range of tens of nanometers.

In this Letter we show that subnanometer-precision SPT can be achieved in 3-D by off-focus imaging of nanoparticles in a standard epifluorescence arrangement. At the expense of precision, particles can also be tracked over large axial distances without the need for sample scanning. The method presented here is practically illustrated in a study of the structure–mobility relationship of a nanoparticle in a polymer network.

In a diffraction-limited wide-field imaging system with numerical aperture NA, the in-focus image of a pointlike object is a spot with a diameter of $\sim 1.22\lambda/\mathrm{NA}$, where λ is the imaging wavelength. With defocus, the spot diameter first increases, and then for larger displacements from the focus complex ring intensity patterns are formed[9] (see Fig. 1). The full 3-D pattern represents the point-spread function of the optical system and is determined mainly by the objective lens.[10] The distance of the object from the imaging focal plane (i.e., axial object position z) is then precisely encoded by the intensity pattern (number and diameter of rings, relative intensity of rings). Much effort has been put into calculating the point-spread function for various microscope arrangements. However, the exact calculation of ring patterns requires, in addition to a rigorous model, knowledge of parameters that are generally not accessible, such as the actual optical properties of the objective lens used. Thus a calculated point-spread function cannot currently serve as the reference basis for subnanometer-precision 3-D SPT, and the actual patterns at different axial positions of the object have to be determined experimentally.

In our experiments we used an epifluorescence setup based on a modified inverted microscope (Axiovert 35, Carl Zeiss) equipped with a high-NA objective lens (Plan Neofluar 100×; oil immersion; NA, 1.3; Carl Zeiss) and a mercury lamp for fluorescence excitation (HBO100, Carl Zeiss). Axial positioning of

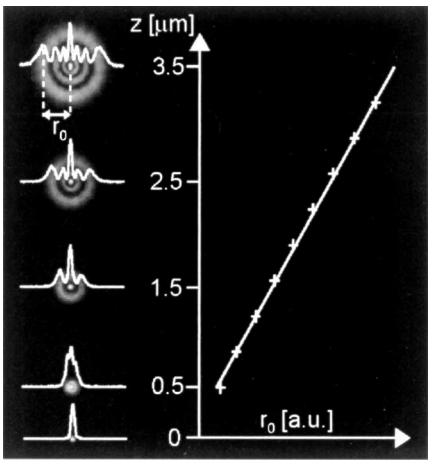

Fig. 1. Images of a 216-nm fluorescent bead embedded in an agarose gel at different distances z from the focal plane (left). In all measurements, actual distances from the focal plane were corrected for refractive-index mismatch between the immersion oil (1.518) and the agarose (1.331).[11] Within the z range (0.5 μm, 3.5 μm), the radius r_0 of the outermost ring in the images scaled linearly with z (right). The bead was fixed $\sim$2 μm above the coverslip surface.

0146-9592/03/020069-03$15.00/0

the imaging focus within the sample was achieved by movement of the objective lens with a piezoactuator (PiFoc P 721, Physik Instrumente), and lateral sample positioning was done with a two-axis piezo-driven stage (NPS-XY-100A, Queenstage Instruments; for details, see Ref. 12). Sample images were recorded with a CCD camera (ORCA-ER, Hamamatsu) and transferred to a computer by use of a frame grabber board (PC Dig, Coreco). Series of images were analyzed off line with custom-written software integrated into IgorPro 4 (Wavemetrics).

To characterize the ring pattern as a function of the object's axial position z, we immobilized 216 ± 8 nm orange fluorescent latex beads (Molecular Probes) in an agarose gel of concentration 1.3% and controlled the amount of defocus by moving the objective lens. Image sequences of beads located at different distances from the coverslip were acquired. A typical result of these experiments is shown in Fig. 1. As the bead is moved away from the focus toward the objective lens (i.e., toward larger z), multiple rings gradually appear in the image, the first at approximately $z = 0.5$ μm. We used radius r_0 of the outermost ring, which contained the major part of the total image intensity [94–75% for the z range (0.5 μm, 3.5 μm)], as a measure of the actual z position. Values of r_0 were extracted from the fits of a rotationally symmetric Gaussian function of the form $f(r) = \exp[-k(r - r_0)^2]$ to the outermost ring. The lateral bead coordinates x, y were then determined from the position of the pattern center in the image. Within the studied z range (0.5 μm, 3.5 μm), r_0 scaled linearly with z (see Fig. 1).

To determine the precision of our particle-tracking algorithm, we modulated the position of an immobilized bead with square waves with peak-to-peak amplitudes of 2 nm in the x direction and 5 nm in the z direction, respectively. The average z position was set to ~1 μm. At this distance, the image contains a single ring with a sharp, well-defined contour. Figure 2(a) shows a typical track of the bead's x position. Steps of 2 nm are clearly visible, and their amplitude is well above the position noise. To determine the error in the position measurement, we calculated the average standard deviation of the bead position during a half-period of the modulation wave when the modulation position was fixed. The resulting value of 0.8 nm was reproduced in independent experiments with beads immobilized at different distances from the coverslip. Figure 2(b) shows a typical track of the bead z position, with the 5-nm steps clearly visible. In this case, the average standard deviation was 0.9 nm. Therefore, the particle position can be measured on subnanometer scale along all three axes.

To investigate how the tracking precision depends on the bead's axial position, at each fixed z we took 20 images of an immobilized bead and calculated the standard deviations of the x, y, and z positions obtained from fits to these images (see Fig. 3). As expected, in the x and y directions, the standard deviations increase monotonically with increasing z. This is caused by spreading of the detected light over more CCD pixels, which is followed by the decrease of the maximum image intensity, I_{max}. Consequently, the ratio of I_{max} to the total detection noise decreases, which degrades the fit stability.[13] The algorithm does not provide any position information in the z direction below $z = 0.5$ μm, because no rings are detectable. After the appearance of the first ring, the z standard deviation initially decreases as the ring contour sharpens. Subsequently, it reaches its minimum value and finally follows the same trend as the x, y data. As implied by Fig. 3, subnanometer precision can be achieved when we are working close to the optimal z position at $z \sim 1$ μm, in

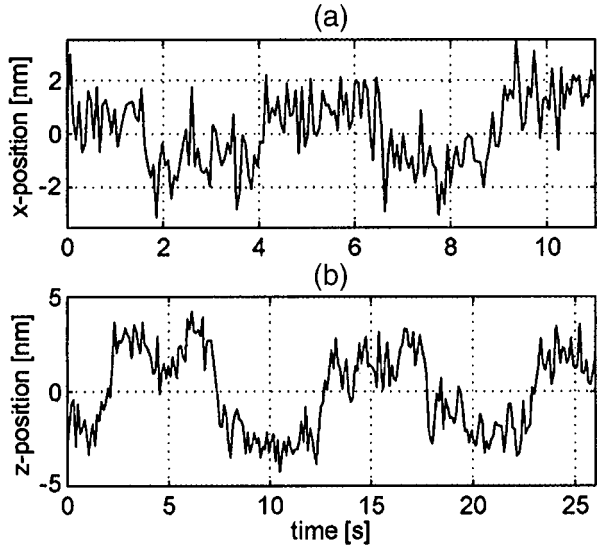

Fig. 2. Position tracking of a 216-nm bead embedded in agarose gel. The bead position was modulated with (a) a square wave of peak-to-peak amplitude 2 nm and period 5 s in the lateral direction and (b) amplitude 5 nm and period 10 s in the axial direction. The average position standard deviations are (a) 0.8 nm (integration time 62 ms) and (b) 0.9 nm (integration time 106 ms). The average z position was 1 μm for both cases.

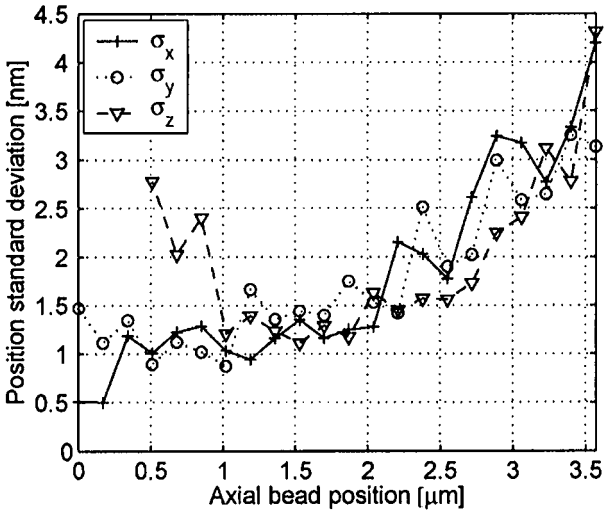

Fig. 3. Precision of the 3-D SPT as a function of the bead's axial position. Single standard deviations σ_x, σ_y, and σ_z of the x, y, and z positions of a stationary 216-nm bead embedded in an agarose gel are shown. The camera integration time for image acquisition was 106 ms. The standard deviations were calculated from 20 data points.

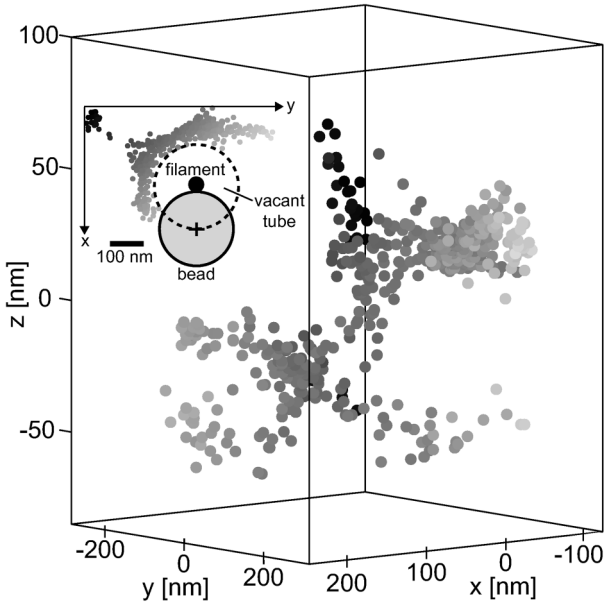

Fig. 4. Hindered diffusion of a 216-nm bead in an agar gel network. The dots represent accessible positions of the bead center; vacant volume elements of tubular shape contain agar filaments (see also inset). The bead position was determined in 2000 successive images containing two to three rings recorded with 7.5 frames/s and integration time of 100 ms. The total volume explored by the beam within the recording time of 267 s was 0.34 μm $\times$ 0.57 μm $\times$ 0.15 μm.

agreement with Fig. 2. However, even for $z = 3.5$ μm, the precision is still better than ± 4 nm.

On the basis of data presented in Fig. 3, it follows that a 216-nm fluorescent bead can be tracked over an axial range of 3 μm with nanometer precision, without adjusting the z position of the sample. Figure 4 illustrates the study of the hindered diffusion of such a bead in an agar gel network, as an example of the application of the 3-D SPT. The low agar concentration permitted bead movement. The 3-D distribution of accessible positions shows strong spatial constrains on the diffusion of the bead, caused by the agar filaments. Thus, this distribution provides information about the structure–mobility relationship. Due to a mechanical amplification effect, the unoccupied volumes resemble tubes with diameter given by the sum of the bead (216 nm) and agar filament diameters (see the inset of Fig. 4). For a tube diameter of $\sim$250 nm, the diameter of the agar filament that creates it is $\sim$34 nm, which is in accordance with previously published data obtained by use of thermal noise imaging in an optical trap.[14]

In conclusion, using a standard epifluorescence microscopy arrangement in an off-focus imaging mode, we have demonstrated the feasibility of 3-D tracking of nanometer-sized particles with subnanometer precision. This precision provides access to molecular dimensions, thus opening a wide range of applications in surface chemistry, polymer physics, colloidal physics, molecular biology, and cell biology. With slightly reduced performance, particles can be tracked over axial intervals of several micrometers without the need of adjusting the axial position. This tracking cannot be achieved with any other high-precision light microscopy technique (e.g., a total internal reflection or a 4-Pi microscope). In our tracking scheme we used only a part of the information contained in a defocused particle image, i.e., the diameter of the outmost ring. By fully exploiting the image, we expect to achieve maximal precision of several tenths of nanometer along all three axes.

The work of A. Jonáš was supported by Deutsche Forschungsgemeinschaft (grant FL 351/1-2). We thank James Swoger and Christian Tischer for discussion and Ernst H. K. Stelzer for additional support. E.-L. Florin's e-mail address is florin@embl-heidelberg.de.

References

1. M. De Brabander, G. Geuens, R. Nuydens, M. Moeremans, and J. De Mey, Cytobios **43,** 273 (1985).
2. M. J. Saxton and K. Jacobson, Annu. Rev. Biophys. Biomol. Struct. **26,** 373 (1997).
3. J. C. Crocker and D. G. Grier, J. Colloid. Interf. Sci. **179,** 298 (1996).
4. R. Yasuda, H. Noji, M. Yoshida, K. Kinosita, Jr., and H. Itoh, Nature **410,** 898 (2001).
5. D. H. Burns, J. B. Callis, G. D. Christian, and E. R. Davidson, Appl. Opt. **24,** 154 (1985).
6. H. P. Kao and A. S. Verkman, Biophys. J. **67,** 1291 (1994).
7. M. Schmidt, M. Nagorni, and S. W. Hell, Rev. Sci. Instrum. **71,** 2742 (2000).
8. C. M. Ajo-Franklin, L. Kam, and S. G. Boxer, Proc. Natl. Acad. Sci. USA **98,** 13643 (2001).
9. S. F. Gibson and F. Lanni, J. Opt. Soc. Am. A **6,** 1357 (1989).
10. D. A. Agard, Y. Hiraoka, P. Shaw, and J. W. Sedat, in *Fluorescence Microscopy of Living Cells in Culture, Part B*, D. L. Taylor and Y. Wang, eds., Vol. 30 of Methods in Cell Biology (Academic, San Diego, Calif., 1989), pp. 353–377.
11. S. Hell, G. Reiner, C. Cremer, and E. H. K. Stelzer, J. Microsc. (Oxford) **169,** 391 (1993).
12. A. Pralle and E.-L. Florin, in *Atomic Force Microscopy in Cell Biology*, B. P. Jena and J. K. H. Hörber, eds., Vol. 68 of Methods in Cell Biology (Academic, San Diego, Calif., 2002), pp. 193–213.
13. N. Bobroff, Rev. Sci. Instrum. **57,** 1152 (1986).
14. C. Tischer, S. Altmann, S. Fisinger, E. H. K. Stelzer, J. K. H. Hörber, and E.-L. Florin, Appl. Phys. Lett. **79,** 3878 (2001).